Article

Railway Track Stress–Strain Analysis Using High-Precision Accelerometers

Alexandr Avsievich [1], Vladimir Avsievich [1], Nikita Avsievich [1], Dmitry Ovchinnikov [2] and Anton Ivaschenko [3,*]

1 Mechatronics, Automation and Transport Control Department, Samara State Transport University, 443066 Samara, Russia; a.avsievich@samgups.ru (A.A.); avsievichv@samgups.ru (V.A.); map@samgups.ru (N.A.)
2 Track Facilities Department, Samara State Transport University, 443066 Samara, Russia; ovchinnikov@samgups.ru
3 Computer Science Department, Samara State Technical University, 443100 Samara, Russia
* Correspondence: vt@samgtu.ru

Featured Application: Diagnostics and monitoring of the railway track lines' infrastructure technical state.

Abstract: We propose a new approach for railway path diagnostics on the basis of track line stress–strain analysis using the data provided by high-precision accelerometers. This type of sensor provides sufficient accuracy with lower costs, and enables the development of a railway digital twin, according to the concept of the Internet of Things. The installation of sensors on a railway track along its entire length allows real-time monitoring of the states of the technical parameters of the railway track, and using mathematical methods to evaluate its wear on the basis of constantly received data. This paper presents an original 3D model of a railway track line and the results of its analysis using a finite element method. To test the model, we performed an analysis of the normal stresses and deformations in the elements of a railway track by simulating the impact of rolling stock on a section of a railway track with intermediate rail fastenings, ZhBR-65SH. The research results were probated and tested at the testing ground of the Kuibyshev branch of Russian Railways, the Samara track. The proposed approach makes it possible to determine the load of the track, and knowing the movement of the rail, to calculate the structural stress in the elements of the railway track, to constantly monitor the parameters of the slope and rail subsidence.

1. Introduction

One of the challenging problems of railway infrastructure monitoring is unmanned track defects diagnostics [1]. At present, the monitoring and control of deformations of the railway track is carried out mainly with the help of a track-testing car, a mobile complex for monitoring the states of technical objects of the railway infrastructure [2,3]. The modern laboratory track-testing car is a fully automated diagnostic complex that can be equipped with a variety of systems in accordance with the customer's requirements.

Despite the many advantages of their use in practice, the implementation of constant monitoring of critical important sections of the railway track remains limited due to increased train traffic. Hence, additional removable measuring instruments are used, equipped with specialized sensor equipment [4,5]. Promising research in this area is related to the implementation of the concept of the Internet of Things [6–8].

A straightforward form of nondestructive railway track testing is carried out using strain gage transducers [9–11]. When applied in practice, it is efficient to use high-precision accelerometers for this purpose. However, this approach requires calculation of

the stress–strain state based on linear displacements. In order to aid the development of this methodology, we propose a new solution based on railway track stress–strain analysis in this paper.

We developed a 3D model of a railway track section, which enabled determination of the impacts of rolling stock on a section of a railway track. Digital modeling of the deformation of the railway track makes it possible to estimate the final mechanical stresses arising in the process of interaction with the rolling stock with a high degree of reliability. Using the input data from digital accelerometers makes it possible to determine the expected movement of the rail and the structural stress in the elements of the railway track. More details are given below.

2. State of the Art

Mechanical deformation arising in the elements of the superstructure of the railway line, and on the main site of the roadbed during the interaction of the track and the rolling stock, are some of the paramount characteristics that determine the durability and economic efficiency of a railway, its life cycle cost, and the safety of the transportation process as a whole [12,13]. Railway track diagnostics are essential for checking the precise condition and evolution of a network's infrastructure; in so doing, they make it possible to formulate a replacement strategy and plan work, taking into account operating requirements.

Most operations in the monitoring and control of deformations of a railway track are currently carried out with the help of various track-testing cars [14,15]. Some examples of this technology's successful use are given in recent papers [16,17]. Nevertheless, the problem of using the sensors deployed on the railway track line remains highly relevant, but does not ensure permanent and reliable monitoring.

Sensors are widely used in the railway industry to perform monitoring of multiple parameters and thus provide high security, reliability, and efficiency. Examples of railway sensors being implemented are presented in [18,19]. Various types of sensors are deployed to provide the required railway track diagnostics [20–22].

Modern ideas, methods, and technological trends in the area of sensor equipment design and development are combined under the concept of the Internet of Things [23–25], which was used as a theoretical basis for the current research. Implementation of this theory in practice is concerned with solving a number of problems of sensor allocation and data collection, which significantly affect the benefits of its application [26,27].

The problem of railway sensor equipment design and development requires simulating a complex system and having access to a railway track and diagnostic instrumentation that dynamically interacts with a rolling stock wheel set in idle and load conditions. In this paper, we propose a new approach for sensor equipment design and development based on a railway track stress–strain analysis [28–30].

The sensors should be located in the places at the most critical risk of construction damage, determined using the stress–strain analysis [31,32]. The stress–strain state of a railway track is mostly influenced by the train load and the configuration of the track's superstructure: the type of rails, intermediate rail fastenings, sleepers, the thickness and compaction of the ballast layer, etc. At present, there is no direct method for determining the mechanical stresses in the elements of the railway track that arise during the action of the rolling stock. However, calculation of the estimated parameters of the internal force factors is possible using classical analytical methods and mathematical numerical modeling.

Railway track line stress–strain state testing has certain specifics that have studied in a number of research projects [33–35]. It is noted that rail stress can be changed due to thermal and mechanical loads in both longitudinal and vertical directions. Therefore, monitoring the longitudinal rail movement or rail creep is regarded as one of the effective ways to understand the rail's stress states in critical locations, including fixed structures such as level crossings, turnouts, and fixed top bridges.

The dynamic component of the design force depends on various factors that must be considered in models and design solutions [36]. Some examples of efficient stress–strain

analysis are illustrated by [37–39], which can be considered in this research. Railway track line monitoring and stress–strain analysis is performed to provide safety and stability according to the modern requirements and standards [40,41]. High longitudinal rail stresses contribute to problems such as track buckling, rail joint failure, rail breakage, and failure of turnouts.

Modeling of a stress–strain state is a separate research area in the railways industry [42–44]. The results of simulation and modeling can be used to determine the characteristics of the railway track and its elements [45,46], in addition to the calculations and real experiments.

The analysis of stresses in the railway elements from the dynamic interference between its parts and operational loads is carried out on basis of the results of finite element modeling [47,48]. The dynamical theory of elasticity enables describing of the dynamic equilibrium of strains of the railway track layers. The model of the stress–strain state for the railway track consists of a combination of the geometric equations of the outline of a part in the system's space involved in interaction at a given time, and the equations of the dynamic equilibrium of its deformation. The modeling process is also used to study the influence of the installation temperature difference on the operational lifetime of the rail.

It is especially noted that the track's substructure is a vital and essential part of the railway system which supports the track, and its properties have a strong influence on the overall track behavior [49]. Analysis of the dynamic interaction between vehicle and railway track considers the complexity of the modeling of the ballast bed, rail pads, under sleeper pads, and their effect on the determination of the overall track stiffness.

As an analytical tool, in this study we implemented the finite element method, which is widely used in academia and industry [50–52]. Some examples of the finite element method being used to analyze complex mechanical systems are presented in [53–55]. The basic premise of the method is that a solution region can be analytically modeled or approximated by replacing it with an assemblage of discrete elements. Since these elements can be put together in a variety of ways, they can be used to represent exceedingly complex shapes.

The finite element method provides stress–strain analysis of a railway track considering the initial and boundary conditions, and also allows taking into account the nonlinear properties of the ballast layer and subgrade soils, while maintaining the calculation accuracy, limited only by the quality of the finite element mesh [56]. With the help of modern mathematical methods, it is possible to monitor the states of all track elements during loading; to study deformations and displacements at any point in the model, which makes it possible to estimate the real rail deflections under the influence of rolling stock wheels; and to study the changes in the rail slope under significant lateral forces.

3. Methods

High-precision accelerometers are currently widely used in technical diagnostics. Being applied for railway track line analysis, they can be installed according to Figure 1. According to this approach, we developed an information-measuring complex for registration and processing of accelerations of elements of the track superstructure and artificial structures under the influence of a dynamic load from the rolling stock. The complex consists of the hardware of 6 three-axis digital accelerometers ACt90 with rail mounting, an MS4812 controller, and a personal computer (see Figure 2).

The proposed complex is intended to determine rail linear displacements in three degrees of freedom. By knowing the type of rolling stock and the corresponding axle load, and measuring the rail movement, it becomes possible to determine the lateral forces acting on the rail from the wheels of the rolling stock, and to establish the parameters of the stress–strain state of the track elements using the equations of approximation and linear interpolation as shown below.
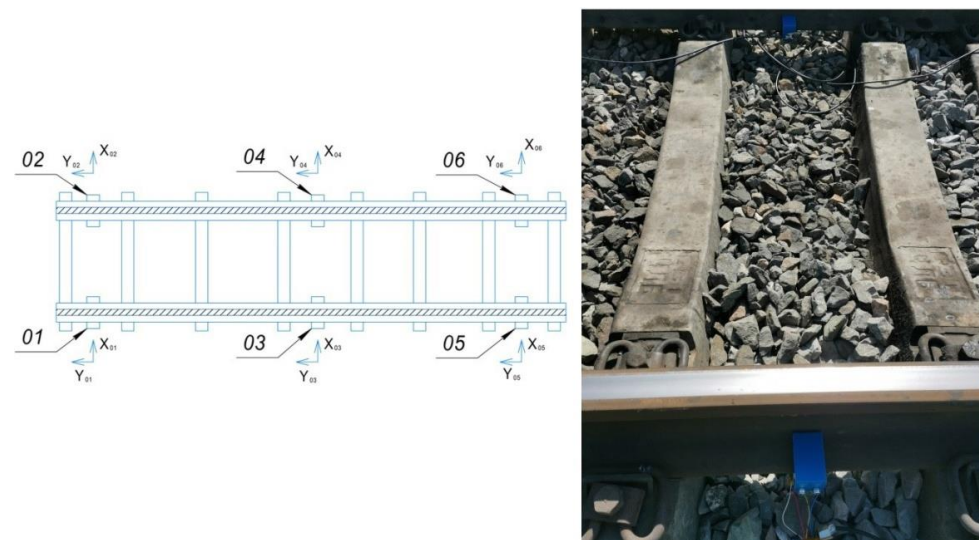
Figure 1. Effective locations of accelerometer sensors on a railway track line.
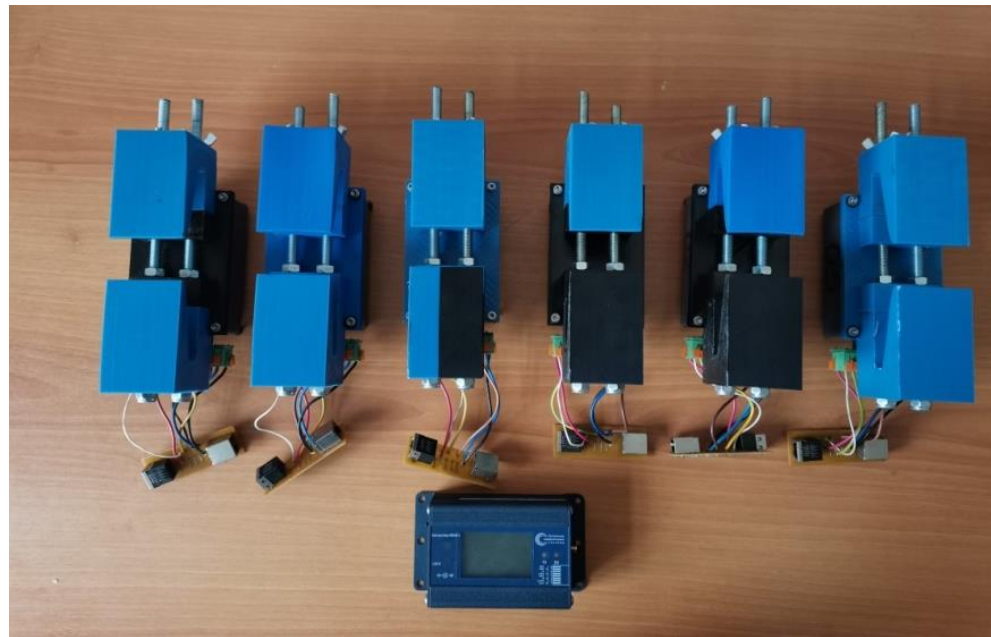

Figure 2. Sensor equipment used for diagnostic instrumentation.

4. Numerical Modeling

In this work, in the environment of finite element modeling software ANSYS, a three-dimensional (3D) model of a section of a railway track was developed, completely repeating the configuration of a real operating track using intermediate rail fasteners of the ZhBR-65Sh type with a rail R65 and crushed stone ballast 45 cm thick under the sleeper (see Figure 3).

On the basis of the 3D model, we developed a finite element model of a railway track (see Figure 4). The details of the 3D model's development and the parameters of the numerical model are presented in [57–59]. The model includes about two million nodes, including the elements of a hexahedral shape, considering the symmetry properties and the specifications of all the necessary contact points and junctions. The model presents the real structure of the railway track line. In places of stress concentration, the size of the element was reduced to achieve the required accuracy of the simulation results.
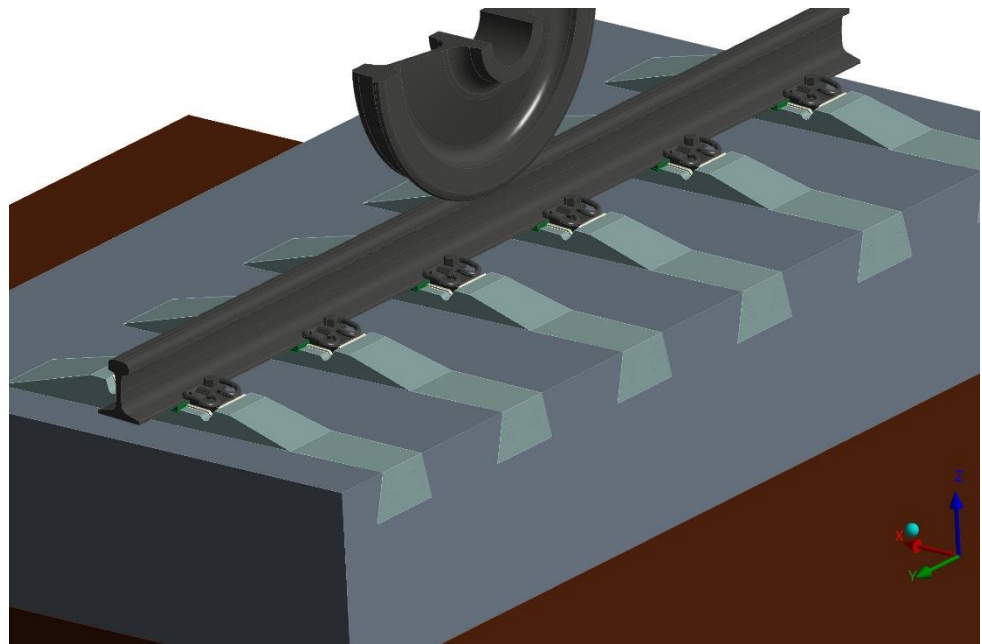
Figure 3. 3D model of a railway track section.
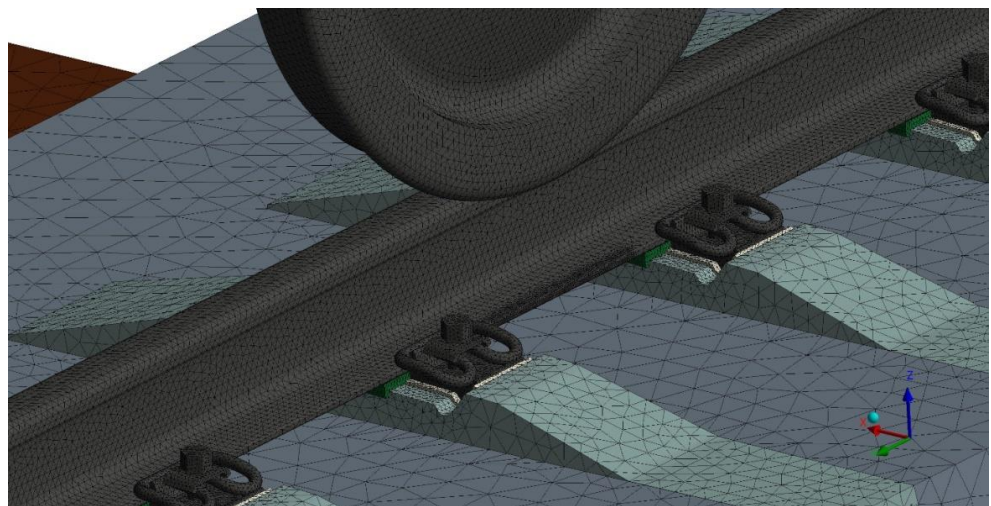
Figure 4. Finite element model of a track section with fasteners of ZhBR-65SH type.

We used both the junctions that allow slight movements of the interacting surfaces, and rigid couplings, depending on each specific case of contact point. Rigid embedding was modeled along the lower plane of the roadbed. The size of the element was selected empirically, taking into account the minimization of the computing time while still achieving the maximum accuracy. In places of stress concentration, the size of the element is reduced to achieve the required accuracy of the results of mathematical modeling.

The initial data for modeling were:

- Rail type R65;
- Ballast prism of a given type of transverse profile;
- The Mohr–Coulomb plasticity model [58] described the nonlinear properties of the layered structure of the ballast prism;
- Rail fasteners of ZhBR-65Sh type;
- Track sections and fastening elements were combined into a solid model;
- Standard tightening of the screws was set to hold the rail in the fasteners;

- The calculated values of the forces on the rails from the rolling stock were formed from the average values observed during the interaction of the track and rolling stocks of different masses when passing sections of different curvature at different speeds: vertical load from 20 to 30 tons per axle, lateral forces from 0 to 10 tons;
- Maximum bending stresses in the rail were determined for the position of the wheel between the two consecutive sleepers.

Loading of the model was carried out in several stages:

1. Tightening of rail fasteners;
2. Application of gravity forces;
3. Exposure of the rolling stock.

It should be noted that the application of loads was implemented not in the form of concentrated forces directed to finite element units and rail elements, but in the form of the forces applied to the wheel of the rolling stock, transmitted to the rail through contact dependencies. This approach enables removing inaccuracies in the calculations caused by an incorrect application of forces to the rail head, excluding additional torque in the section of interaction between the rail and the wheel.

5. Analysis

The results of modeling the impact of rolling stock on a section of a railway track with intermediate rail fastenings ZhBR-65SH are presented below in the form of contours of normal stresses and deformations in the elements of the railway track (see Figures 5–8 and Table 1). The axial load was 30 ton-force (tf), and the lateral force was 10 tf.

As can be seen from the figures, the highest stress was in the Y direction longitudinally. The side stresses were more important for the control of destructive effects.

The data presented in Table 1 enabled determination of the boundaries of rail movements dependent on vertical and side forces. Approximations of these simulation results provided the dependences of the lateral forces acting on the rail on the magnitude of the displacements at various axial loads (see Figure 9):

$$y = -126.066x^2 + 418.748x - 231.351, R^2 = 1.0;$$
$$y = -191.104x^2 + 615.992x - 391.266, R^2 = 1.0;$$
$$y = -246.606x^2 + 829.830x - 596.294, R^2 = 1.0$$

where x—displacement in mm.
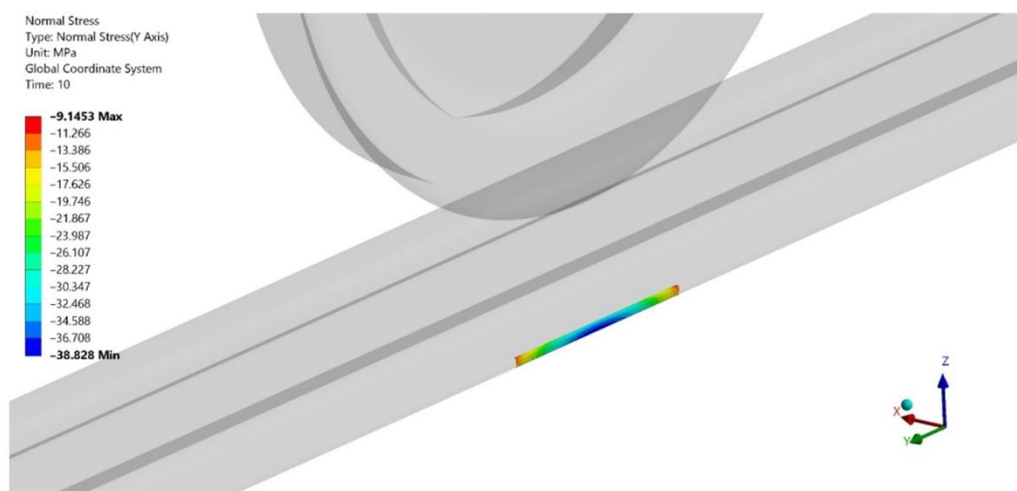
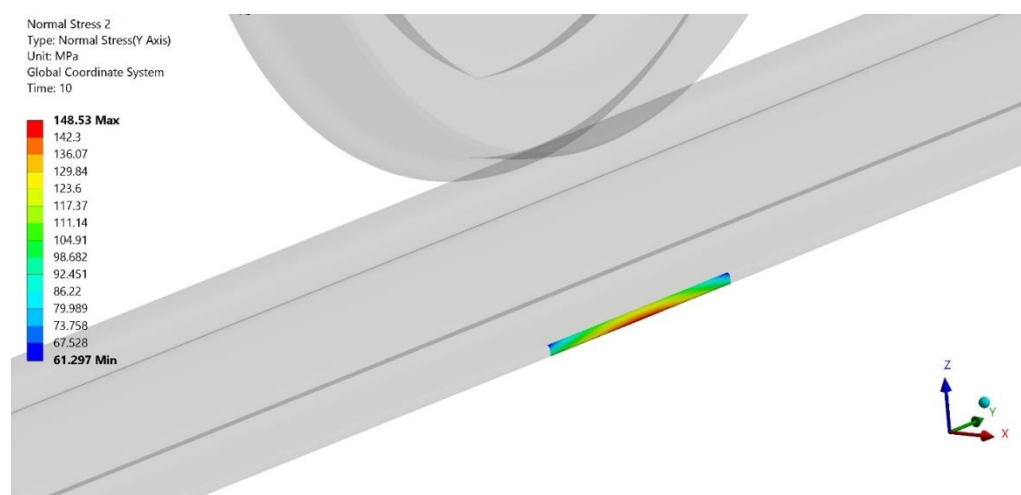**Figure 5.** Bending stresses on the inner edge of the rail.

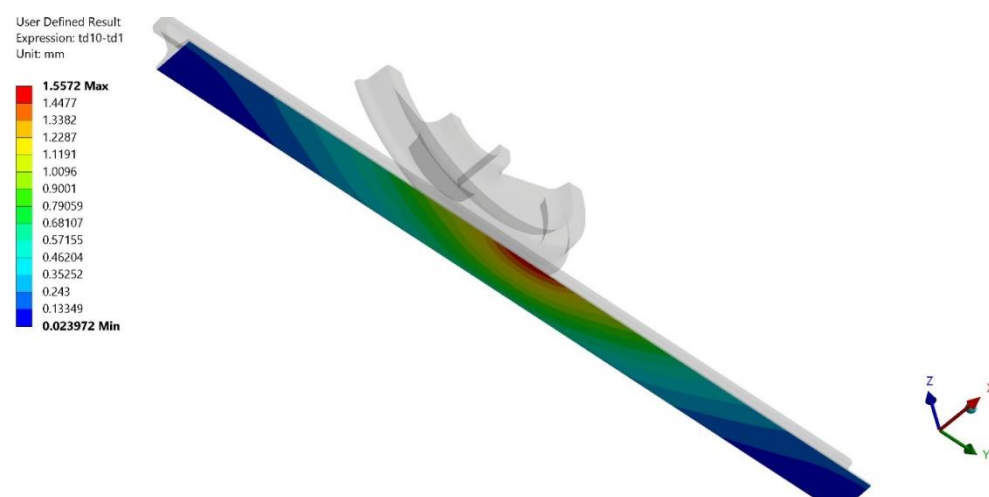**Figure 6.** Bending stresses on the outer edge of the rail.

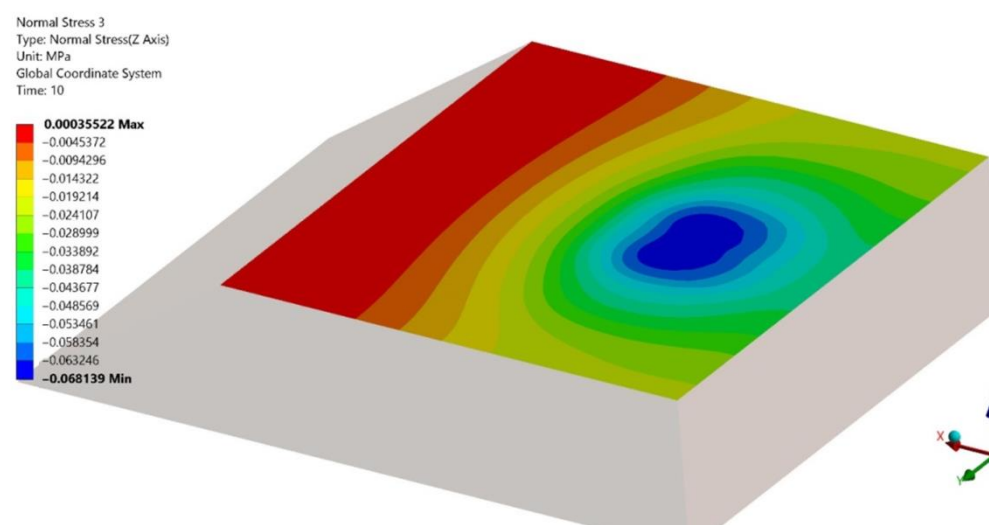**Figure 7.** Movement of a rail under the influence of a train load.

Figure 8. Stresses at the main site of the subgrade.

Table 1. Simulation results under loading of a track section [1].

Vertical Wheel Force, kN	Side Force, kN	Inner Sole Edge	Outer Sole Edge	Moving the Rail (Wheel between the Sleepers)	Subgrade (Wheel between the Sleepers)
98.1	0	43.88	31.29	0.7	−0.04787
98.1	49.05	2.341	82.409	0.93	−0.047068
98.1	98.1	−18.344	133.28	1.28	−0.049891
122.63	0	54.495	39.002	0.87	−0.057487
122.63	49.05	10.511	90.069	1.07	−0.05667
122.63	98.1	−13.764	140.91	1.42	−0.058574
147.15	0	65.134	46.598	1.04	−0.067109
147.15	49.05	18.719	97.654	1.22	−0.066353
147.15	98.1	−9.1453	148.53	1.56	−0.068139

[1] Normal stresses, MPa; displacement, mm; 1840 shp/km; ballast, 45 cm.
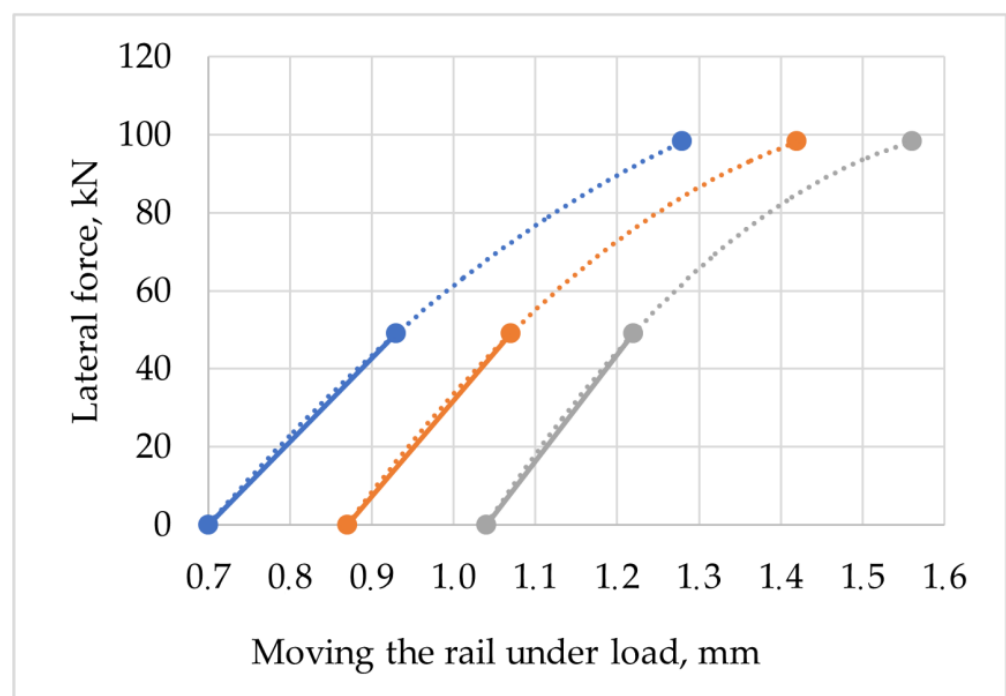
Figure 9. Restored side forces acting on the rail for the corresponding rail movements at various axial loads.

The coefficient of accuracy of the approximation was equal to one, which indicated the maximum degree of compliance of the trend model with the initial data.

There was an obvious dependence of the increase in the growth of displacements with the addition of lateral forces for certain axial loads.

Thus, knowing the type of rolling stock with the corresponding axle load, and by measuring the rail movement, it was possible to determine the lateral forces acting on the rail from the wheels of the rolling stock, and to establish the parameters of the stress–strain state of the track elements using the equations of approximation and linear interpolation.

The corresponding rail deflections are presented in Figure 10. Using high-precision accelerometers with the distance between the sensors 1.5–2 m, it was possible to obtain the maximum and minimum values of the deflections on adjacent sensors.
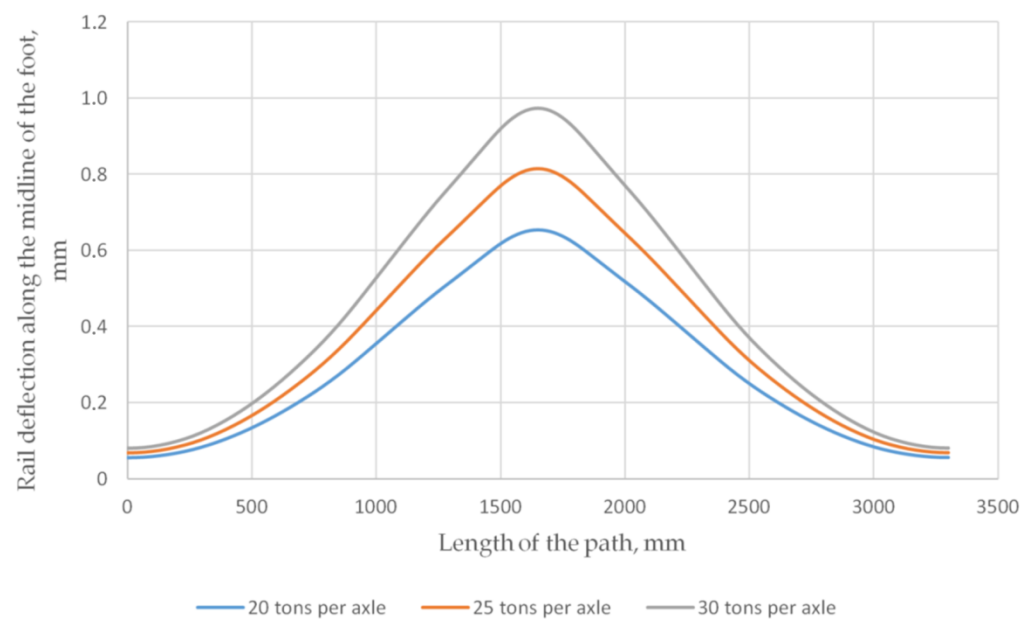
Figure 10. Deflection of the midline rail of the sole under different loads.

Therefore, the proposed approach is suitable for studying the deflections of one rail, and the influences of adjacent wheels of the carriage bogie. Simulation results are presented in Table 2.

Table 2. Simulation results.

Simulation Step	Vertical Wheel Force, kN	Lateral Force, kN	Inner Sole Edge	Outer Sole Edge	Moving the Rail (Wheel between Sleepers)	Subgrade (Wheel between Sleepers)
1	98.100	49.050	2.341	82.409	0.930	−0.047
1	98.100	61.330	−2.838	95.145	1.000	−0.048
1	98.100	98.100	−18.344	133.280	1.280	−0.050
2	122.630	0.000	54.495	39.002	0.870	−0.057
2	122.630	33.620	24.347	74.004	1.000	−0.057
2	122.630	49.050	10.511	90.069	1.070	−0.057
3	98.100	61.330	−2.838	95.145	1.000	−0.048
3	110.400	47.435	10.794	84.545	1.000	−0.052
3	122.630	33.620	24.347	74.004	1.000	−0.057
Final state	110.400	47.435	10.794	84.545	1.000	−0.052

That is, for example, when a coach with a mass of 90 tons passed (corresponding to a wheel load of 110.4 kN) and the rail moved directly under the wheels of a rolling stock 1 mm in size, the resulting forces and stresses were calculated in several stages:

1. The wheel load of 110.4 kN was between 98.1 and 122.63 kN (step 1);
2. A moving rail magnitude of 1 mm corresponds to lateral forces under an axial load of 98.1 kN, equal to: $-126.066 \cdot x^2 + 418.748 \cdot x - 231.351$. Lateral forces were defined as 61.33 kN (step 3);
3. Movement of rail magnitude of 1 mm corresponds to lateral forces at 122.63 kN, axial load equal to: $-191.104 \cdot x^2 + 615.992 \cdot x - 391.266$. Lateral forces were measured at 33.62 kN (step 4);
4. With the help of linear interpolation, we determined the stress–strain state of the elements of the railway track at a wheel load of 110.4 kN and the occurrence of rail displacements directly under the wheels of the rolling stock of 1 mm in size (final step).

6. Experiments

The presented results were probated on the testing ground of the Kuibyshev branch of Russian Railways, the Samara track distance, using the set of high-precision accelerometers. The sensors were installed according to the diagram presented above.

As a result of measurements, vibration (acceleration) data were obtained from the results of the passage of two passenger trains and two freight trains. According to the simulation, the distance between the sensors for two passenger trains and the first freight train was set to 1.5 m. For the second freight train, the distance between the sensors was increased to 5 m, to test the hypothesis about the influence of the wheel sets of one car on the wheel set of the other. The distance between the wheel sets for all types of cars was on average 10.23 m.

The data on the impact of freight and passenger trains on the railway track are presented in Figures 11 and 12. The figures present the acceleration data obtained from sensors installed on the rail under the dynamic impacts of freight and passenger trains on the railway track, based on the first sensor. The maximum amplitude of the track acceleration of freight trains was 41 m/s^2 on the first sensor on the vertical (*z*-axis), and that of passenger trains was 23 m/s^2, which corresponds to the actual condition, since the mass of freight train cars is higher than that of passenger trains. This parameter characterizes the vertical forces acting on the track under the influence of the mass of the wheel set acting on the axle.

The maximum amplitude of the lateral acceleration of freight trains on the rail (*x*-axis) was 21 m/s^2, and that of passenger trains was 9 m/s^2, which characterizes the lateral effect of the wheel set on the rail under the action of forces arising from irregularities in the track and centrifugal forces on the turning sections of the track. The longitudinal maximum rail acceleration (*y*-axis) of freight trains is 10 m/s^2, and that of passenger trains is 7 m/s^2, which characterizes the action of forces arising from the rolling of the wheel onto the rail and depends on the speed and mass of the train.

The obtained acceleration results correspond to the real state, since the mass of freight train cars is higher than that of passenger trains.

To check the linear relationship between the sensors, the correlation coefficients were calculated for each axis separately (see Tables 3–5). The analysis of the coefficients of cross-correlation between the sensors did not reveal a linear relationship between them. The influence of the design features of the cars on the acceleration was not found.
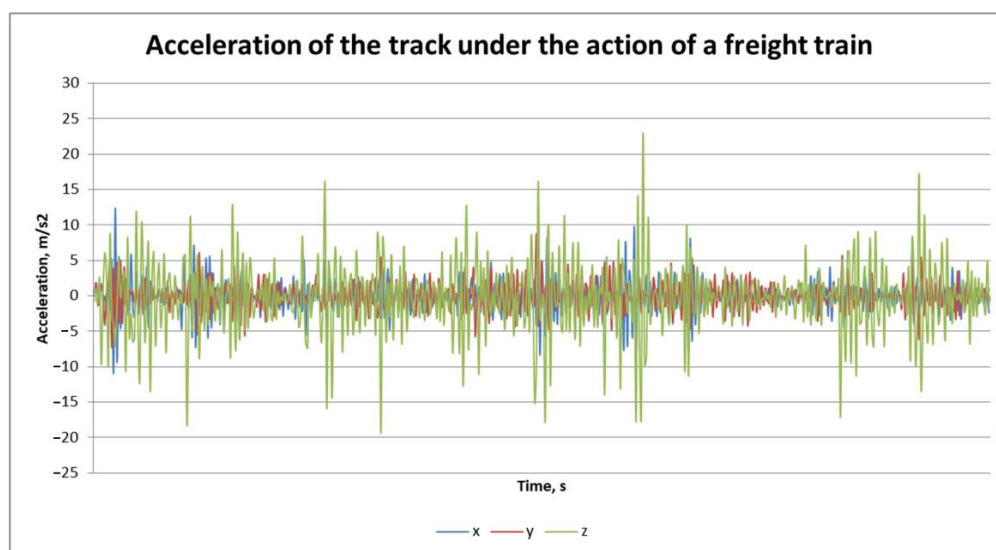
Figure 11. Acceleration of the track along the axes under the action of a freight train on the first sensor.
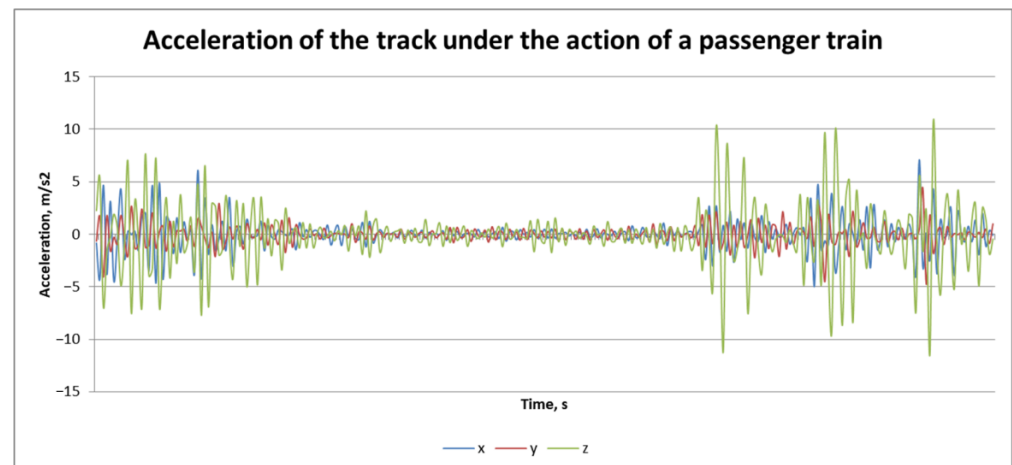
Figure 12. Acceleration of the track along the axes under the action of a passenger train on the first sensor.

Table 3. Matrix of correlation coefficients between sensors' axis X.

Vertical Wheel Force, kN	Lateral Force, kN	Inner Sole Edge	Outer Sole Edge	Rail Movement	Subgrade
1	0.03811	0.114333	0.102891	−0.01411	0.010177
	1	0.00582	0.120959	−0.01244	−0.02912
		1	0.274156	−0.11147	−0.00882
			1	0.057253	0.024453
				1	−0.1091
					1

Table 4. Matrix of correlation coefficients between sensors' axis Y.

| Vertical Wheel Force, kN	Lateral Force, kN	Inner Sole Edge	Outer Sole Edge	Rail Movement	Subgrade
1	0.092505	0.030213	0.040231	0.041666	−0.01078
	1	0.048245	−0.00705	0.014493	−0.0382
		1	−0.34413	0.083251	−0.09929
			1	−0.04389	−0.00759
				1	0.27666
					1

Table 5. Matrix of correlation coefficients between sensors' axis Z.

Vertical Wheel Force, kN	Lateral Force, kN	Inner Sole Edge	Outer Sole Edge	Rail Movement	Subgrade
1	−0.04647	−0.02142	0.007001	−0.02553	0.010177
	1	0.069503	−0.10857	−0.02469	0.011199
		1	−0.08434	−0.04817	0.126454
			1	−0.00148	0.007194
				1	−0.24768
					1

From the obtained data, using double integration, a dynamic deviation from the equilibrium position was obtained at the first sensor (see Figures 13 and 14), showing that the rail subsidence under the influence of vertical forces (*z*-axis) of the freight train was within 6 mm, when the amplitude of the rail oscillation was within 9 mm. In this case, the subsidence under the passenger train was within 1.8 mm, and the vibration amplitude did not exceed 4.5 mm, which is within the values obtained using the modeling process.
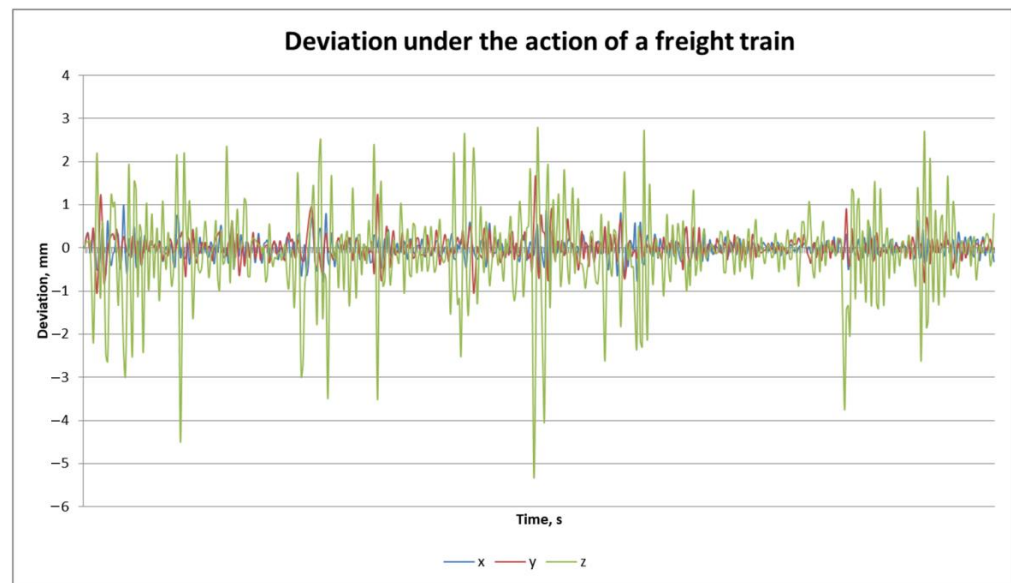
Figure 13. Deviation of the track along the axes under the action of freight train on the first sensor.
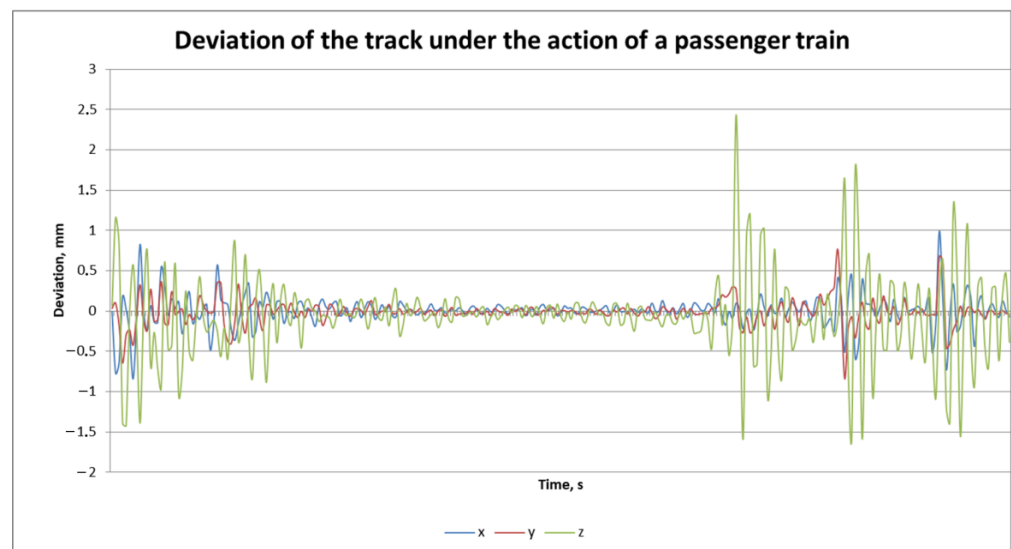
Figure 14. Deviation of the track along the axes under the action of passenger trains on the first sensor.

The impact of lateral forces of freight trains deviates the path from the initial state by a maximum of 1 mm, with a vibration amplitude of 1.3 mm. Passenger trains arouse the maximum deviation of 1 mm, with a vibration amplitude of 1.7 mm. The results obtained for vertical and lateral deviations are within the values calculated using the simulation results. Deviations from the position of the initial sensor installation in the longitudinal direction (*y*-axis) caused by a freight train were at most 1 mm. The maximum oscillation amplitude was 1.3 mm. The maximum deviation caused by a passenger train was 1 mm with an oscillation amplitude of 1.8 mm.

As can be seen from these results, the rolling stock acts on the track so that the track's movement is observed simultaneously in three directions. By fixing these parameters in a constant mode, it becomes possible to monitor the technical parameters of the track, and as a consequence, to identify the deviations from the technical regulations for track maintenance in advance.

Compared with the real railway track deviations (calculated using the acceleration data) resulting from passenger and freight trains, the values calculated as the result of

modeling are in good agreement. This fact proves the possibility of using high-precision accelerometers for railway track stress–strain analysis.

7. Discussion

Verification of the developed model was carried out using the methodology for assessing the impact of rolling stock on the track according to the conditions for ensuring reliability, approved by order of JSC Russian Railways Number 2706r, dated 22 December, 2017. The initial data include the characteristics of the stiffness of the rail base and the rail, the elasticity of the rail base, and the equivalent load determined with regard to them. These parameters consider the maximum forces transmitted from the wheel to the rail, taking into account the elastic deflection of the rail in the places where the vertical forces from the adjacent wheels are concentrated.

The assessment of the vertical deflection of the rail during the passage of various types of rolling stock is presented in Table 6. In the first approximation, the value of the force transmitted from the wheel is taken to be equal to the static load. The modulus of elasticity of the rail base for a railway track with R65 rails on reinforced concrete sleepers with a diagram of 1840 sp./Km is about 150 MPa.

Table 6. Theoretical parameters of rail deflections.

Rolling Stock	Number of Axles in the Bogie	Force Transmitted from the Wheel to the Rail, kN	Distance between the Axles of the Wheels, m	Equivalent Load, kN	Vertical Rail Deflection, mm
Passenger locomotive	3	105.5	2.90	104.00	0.53
Passenger coach	2	78.5	2.40	75.80	0.39
Freight locomotive	2	112.8	3.00	111.56	0.57
Freight car	2	122.6	1.84	117.95	0.60

Therefore, the results of finite element modeling and the experiments correspond to the calculated values of deflection, taking into account the idealization and simplification of the theoretical solution of loading a railway track. In fact, the vertical displacements exceed the calculated values due to dynamic impacts of wheels with sliders on the rails, and the presence of an unconsolidated ballast layer under the sleepers, which is clearly seen in the graphs of the results of experimental studies.

Experimental rail deviations under the action of a freight train with 122.6 kN axle force allowed calculating the lateral forces (see Figure 15). As it can be seen from the figure, they are coincident with the presented results of modeling and approximation.

With the help of the developed system, it is possible to control both static and dynamic rail inclination during the passage of the rolling stock by determining the angle of inclination of the rail base by the expression:

$$\alpha = arctg\left(\frac{A_x}{A_z}\right), \tag{1}$$

where A_x and A_z are the values of static acceleration along the x and z axes.

The proposed approach of high-precision accelerometers installation on the basis of the railway track line stress–strain analysis makes it possible to determine the load of the track; and knowing the movement of the rail, it becomes possible to calculate the stress in the elements of the railway track, to constantly monitor the parameters of the slope and rail subsidence.

Determination of rail displacements with discreteness of at least tenths of a millimeter, in tandem with the use of a digital model of the deformation of the railway track, makes it possible to estimate the final mechanical stresses arising in the process of interacting with rolling stock with a high degree of reliability. In addition to that, the proposed method of

monitoring of the railway track's vertical and side deviations enables identification of a ground failure or a malfunction of a large number of rail fasteners in a short period of time.

The equation shown on the chart:
$$y = -191.104x^2 + 615.992x - 391.266$$
$$R^2 = 1.000$$
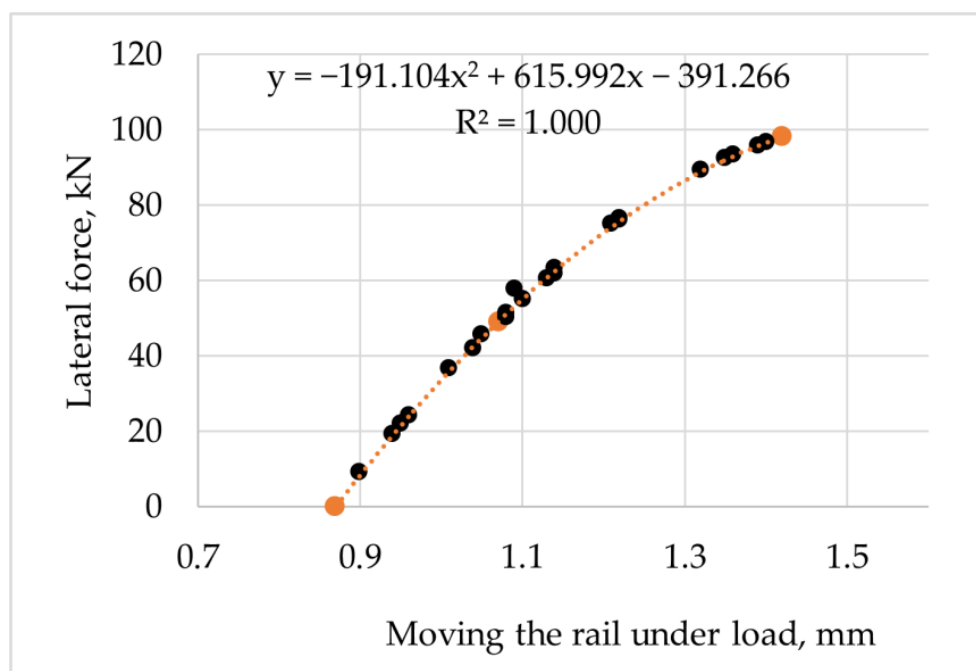
Figure 15. Experimental side forces for the corresponding rail movements.

The concept of the Internet of Things potentially allows increasing the efficiency of railway infrastructure monitoring for track defects diagnostics. Its implementation in practice is associated with expansion and diversity of types of sensors used, giving preference to the easiest to use, cheapest, and most reliable analogs.

With this in mind, the currently widely used mobile laboratory cars should be supplemented with sensors placed directly on the track sections, which allow for regular monitoring, regardless of high train traffic. Typical strain gage transducers are suitable for these purposes, but are difficult to install and operate, especially with large temperature fluctuations.

Using high-precision accelerometers is preferable in terms of operating factors, but requires a transition from measuring rail track deviations to stress–strain analysis. As shown above, a specifically developed finite element model of a railway track provides the means for such a changeover. Our experimental results showed coincidence of observed deviations with the corresponding vertical and side forces acting on the rail under various axial loads.

8. Conclusions

The proposed approach of a diagnostic sensor system on the basis of railway track stress–strain analysis provides a new means for path diagnostics using the Internet of Things, in addition to mobile laboratories. Installation of sensors on a railway track along its entire length will allow real-time monitoring of the states of its technical parameters, and the use of mathematical methods to evaluate its wear on the basis of constantly received data.

A significant deviation in the value of the dynamic bias from the parameters of the static states of the elements of the superstructure of the railway track makes it possible to identify areas with deviations from the norms for the content of rail fastenings, leading to the outstretching of the rail when interacting with the wheels of the rolling stock, and to detecting areas with increased lateral forces. An increase in lateral forces leads to lateral contact between the wheel and rail, increased wear, and as a result, a shorter life cycle.

Thus, the determination of such sections is an important task of track maintenance, to increase the service lives of railway track superstructure elements.

Author Contributions: Conceptualization, A.A. and A.I.; methodology, D.O.; software, V.A. and N.A.; validation, D.O.; investigation, V.A., N.A. and D.O.; writing—original draft preparation, A.A. and D.O.; writing—review and editing, A.I.; project administration, A.A. All authors have read and agreed to the published version of the manuscript.

Conflicts of Interest: The authors declare no conflict of interest.

References

1. Pirvan, A.I.; Patru, G.C.; Tranca, D.C.; Contasel, C.; Rosner, D. Infrastructure independent rail quality diagnosis and monitoring system. In Proceedings of the 18th RoEduNet Conference: Networking in Education and Research (RoEduNet), Galați, Romania, 10–12 October 2019; pp. 1–5.
2. Waston, P.F.; Ling, C.S.; Roberts, C.; Goodman, C.J.; Li, P.; Goodall, R.M. Monitoring vertical track irregularity from in-service railway vehicles. *Rail Rapid Transit* **2007**, *221*, 75–88. [CrossRef]
3. Tsunashima, H.; Matsumoto, A.; Mizuma, T.; Mori, H.; Naganuma, Y. Condition monitoring of railway track using in-service vehicle. *J. Mech. Syst. Transp. Logist.* **2012**, *3*, 154–165.
4. Falamarzi, A.; Moridpour, S.; Nazem, M. A review on existing sensors and devices for inspecting railway infrastructure. *J. Kejuruter. J. Eng.* **2019**, *31*, 1–10.
5. Karthikamani, R.; Kumar, R.; Divya, N. Application of sensors in railway tracks for safety. *Int. J. Recent Technol. Eng.* **2019**, *7*, 75–77.
6. Hodge, V.J.; O'Keefe, S.; Weeks, M.; Moulds, A. Wireless sensor networks for condition monitoring in the railway industry: A survey. *IEEE Trans. Intell. Transp. Syst.* **2015**, *16*, 1088–1106. [CrossRef]
7. Balo, F.; Torğul, B. Internet of Things: A survey. *Int. J. Appl. Math. Electron. Comput.* **2016**, *2016*, 104–110.
8. Patel, K.; Patel, S.; Scholar, P.; Salazar, C. Internet of Things-IOT: Definition, characteristics, architecture, enabling technologies, application & future challenges. *Int. J. Eng. Sci. Comput.* **2016**, *6*, 6122–6131.
9. Liu, G.; Liu, H.; Wei, A.; Xiao, J.; Wang, P.; Li, S. A new device for stress monitoring in continuously welded rails using bi-directional strain method. *J. Mod. Transp.* **2018**, *26*, 179–188. [CrossRef]
10. Yu, F.; Hendry, M. A new strain gauge configuration on the rail web to decouple the wheel–rail lateral contact force from wayside measurement. *Proc. Inst. Mech. Eng. Part F J. Rail Rapid Transit* **2019**, *233*, 095440971882287. [CrossRef]
11. Tutak, P. Application of strain gauges in measurements of strain distribution in complex objects. *J. Appl. Comput. Sci. Methods* **2014**, *6*, 135–145. [CrossRef]
12. Li, C.; Wang, P.; Gao, T.; Wang, J.; Yang, C.; Liu, H.; He, Q. Spatial–temporal model to identify the deformation of underlying high-speed railway infrastructure. *J. Transp. Eng. Part A Syst.* **2020**, *146*, 04020084. [CrossRef]
13. Gou, H.; Xie, R.; Liu, C.; Bao, Y.; Pu, Q. Analytical study on high-speed railway track deformation under long-term bridge deformations and interlayer degradation. *Structures* **2021**, *29*, 1005–1015. [CrossRef]
14. Stow, J.; Andersson, E. Field testing and instrumentation of railway vehicles. In *A Handbook of Railway Vehicle Dynamics*; CRC Press: Boca Raton, FL, USA, 2006; pp. 423–456.
15. Wang, M.; Cai, C.; Zhu, S.; Zhai, W. Experimental study on dynamic performance of typical nonballasted track systems using a full-scale test rig. *Proc. Inst. Mech. Eng. Part F J. Rail Rapid Transit* **2016**, *231*, 470–481. [CrossRef]
16. Presle, G.; Hanreich, W.; Mittermayr, P. Austrian track testing and recording car EM 250: Source for wheel-rail interaction analysis. *Transp. Res. Rec.* **2000**, *1713*, 22–28. [CrossRef]
17. Tasaka, H. Overview of N700S confirmation testing car. *Jpn. Railw. Eng.* **2019**, *203*, 1–4.
18. Lenart, M.; Bielecki, A.; Lesot, M.; Petrisor, T.; d'Allonnes, A. Trust dynamics: A case-study on railway sensors. In Proceedings of the 8th International Conference on Sensor Networks, Prague, Czech Republic, 26–27 February 2019; pp. 47–57.
19. Camci, F.; Eker, Ö.; Baskan, S.; Konur, S. Comparison of sensors and methodologies for effective prognostics on railway turnout systems. *Proc. Inst. Mech. Eng. Part F J. Rail Rapid Transit* **2016**, *230*, 24–42. [CrossRef]
20. Jovanović, D.; Milenković, B. The use of fbg sensors in smart railway. In Proceedings of the IEEE STEC-13th Student Project Conference ESTEC-13, Smolenice, Slovakia, 11 October 2020.
21. Zhang, S.; Lee, W.-K.; Pong, P. Train detection by magnetic field sensing. *Sens. Mater.* **2013**, *25*, 423–436.
22. Machu, Z.; Ksica, F.; Hadas, Z.; Kratochvilova, M.; Podrouzek, J. Sensing rail system with piezoelectric elements. *MM Sci. J.* **2021**, *2021*, 4230–4237. [CrossRef]
23. Farooq, M.; Waseem, M.; Mazhar, S.; Khairi, A.; Kamal, T. A review on Internet of Things (IoT). *Int. J. Comput. Appl.* **2015**, *113*, 1–7.

24. Wortmann, F.; Flüchter, K. Internet of Things. *Bus. Inf. Syst. Eng.* **2015**, *57*, 221–224. [CrossRef]

25. Farhan, L.; Kharel, R.; Kaiwartya, O.; Quiroz, M.; Alissa, A.E.; Abdulsalam, M. A concise review on Internet of Things (IoT)—Problems, challenges and opportunities. In Proceedings of the 11th International Symposium on Communication Systems, Networks, and Digital Signal Processing (CSNDSP 2018), Budapest, Hungary, 18–20 July 2018.

26. Bessis, N.; Dobre, C. Big Data and Internet of Things: A roadmap for smart environments. In *Studies in Computational Intelligence*; Springer: New York, NY, USA, 2014; 450p.

27. Fortuno, G.; Trunfio, P. *Internet of Things Based on Smart Objects: Technology, Middleware and Applications*; Springer: New York, NY, USA, 2014; 250p.

28. Krutko, A.; Sedykh, D.; Vorobev, A.; Putintseva, A.; Filippov, Y. Study of stress-strain state of wheelset of freight car during braking. *Omsk. Sci. Bull.* **2019**, *1260*, 15–19. [CrossRef]

29. Abdurashitov, A.Y.; Sychev, V.P. Evaluation of the strain-stress condition of rails. *IOP Conf. Ser. Mater. Sci. Eng.* **2020**, *760*, 012001. [CrossRef]

30. Umanskii, A.; Yur'ev, A.; Dorofeev, V.; Dumova, L. Stress-strain state of metal at the initial stage of railway rails rolling. *Izvestiya. Ferr. Metall.* **2021**, *64*, 550–560. [CrossRef]

31. Ovchinnikov, D.; Kovenkin, D. Stress-strain state of the "wheel-rail" system under different movement conditions. *IOP Conf. Ser. Mater. Sci. Eng.* **2021**, *1151*, 012020. [CrossRef]

32. Telipko, L.; Mamaev, L.; Raksha, S. The subgrade heterogeneity consideration of a railway track when determining its stress-strain state. Science and Transport Progress. *Bull. Dnipropetr. Natl. Univ. Railw. Transp.* **2018**, *6*, 101–117. [CrossRef]

33. Kluchnik, S. Stress-strain state of beam staged connection point of the railway bridge track-way. Science and transport progress. *Bull. Dnipropetr. Natl. Univ. Railw. Transp.* **2017**, *3*, 160–170. [CrossRef]

34. Nafis, A.; Shah, S.; Mandal, N.; Chattopadhyay, G.; Powell, J.; Micenko, P. Improvement of rail creep data to measure the stress state of a tangent continuously welded rail (CWR) track. In Proceedings of the International Heavy Haul Association Conference, Calgary, AB, Canada, 19–22 June 2011.

35. Kolos, A.F.; Petrova, T.M.; Makhonina, A.O. Full-scale study of stress-strain state of ballastless upper structure construction of rail way in terms of train dynamic load. *Procedia Eng.* **2017**, *189*, 429–433. [CrossRef]

36. Kurhan, D. Determination of load for quasi-static calculations of railway track stress-strain state. *Acta Tech. Jaurinensis* **2016**, *9*, 83–96. [CrossRef]

37. Barabash, M.; Bashinsky, Y.; Korjakins, A. Stress-strain state of the structure in the service area of underground railway. *IOP Conf. Ser. Mater. Sci. Eng.* **2017**, *251*, 012100. [CrossRef]

38. Semenov, A.; Poryvaev, I.; Akhmetdinova, G. Analysis of the stress-strain state of the Forth Rail Bridge structures. *Russ. J. Transp. Eng.* **2016**, *3*, 3. [CrossRef]

39. Kozlov, I. Stress-strain state of railway embankment with the use of mineral geoecoprotective material. *Lect. Notes Civ. Eng.* **2020**, *1*, 287–293. [CrossRef]

40. Nafis, A.; Shah, S.; Mandal, N.; Chattopadhyay, G.; Powell, J. Development of a unified railway track stability management tool to enhance track safety. *Proc. Inst. Mech. Eng. Part F J. Rail Rapid Transit* **2013**, *227*, 493–516.

41. Potvin, M.; Trizotto, M.; Dersch, M.; Edwards, J.; Lima, A. A review of parameters affecting rail break gap size using analytical methods. In Proceedings of the Joint Rail Conference, Virtually, 20–21 April 2021.

42. Prokopev, V.; Zhdanova, T.; Kushkhov, B. Modeling of the stress-strain state of railway wheel and rail in contact. In *Advances in Intelligent Systems and Computing*; Springer: New York, NY, USA, 2020; Volume 982, pp. 603–614.

43. Muravev, V.; Tapkov, K.; Volkova, L.; Platunov, A. Strain stress model of the rail with crack in its head and estimation of its operational lifetime. *Mater. Sci. Forum* **2019**, *970*, 177–186. [CrossRef]

44. Muravev, V.; Tapkov, K. Evaluation of strain-stress state of the rails in the production. *Devices Methods Meas.* **2017**, *8*, 263–270. [CrossRef]

45. Snitko, S.; Yakovchenko, A.; Gorbatyuk, S. Accounting method for residual technological stresses in modeling the stress-deformed state of a railway wheel disk. Report 1. *Izvestiya. Ferr. Metall.* **2021**, *64*, 337–344. [CrossRef]

46. Kurhan, D.; Kurhan, M. Modeling the dynamic response of railway track. *IOP Conf. Ser. Mater. Sci. Eng.* **2019**, *708*, 012013. [CrossRef]

47. Giannella, V. Stochastic approach to fatigue crack-growth simulation for a railway axle under input data variability. *Int. J. Fatigue* **2020**, *1144*, 106044. [CrossRef]

48. Giannella, V.; Sepe, R.; Borrelli, A.; De Michele, G.; Armentani, E. Numerical investigation on the fracture failure of a railway axle. *Eng. Fail. Anal.* **2021**, *129*, 105680. [CrossRef]

49. Shaltout, R.; Ulianov, C.; Chen, H.M. Coupled numerical modelling of railway track substructure with vehicle-track interaction. *Civ.-Comp. Proc.* **2015**, *108*. [CrossRef]

50. Erhunmwun, I.; Ikponmwosa, U. Review on finite element method. *J. Appl. Sci. Environ. Manag.* **2017**, *21*, 999. [CrossRef]

51. Jagota, V.; Sethi, A.; Kumar, D.K. Finite element method: An overview. *Walailak J. Sci. Technol.* **2013**, *10*, 1–8.

52. Cen, S.; Li, C.F.; Rajendran, S.; Hu, Z. Advances in finite element method. *Math. Probl. Eng.* **2014**, *2014*, 206369. [CrossRef]

53. Shlyannikov, V.; Yarullin, R.; Yakovlev, M.; Giannella, V.; Citarella, R. Mixed-mode crack growth simulation in aviation engine compressor disk. *Eng. Fract. Mech.* **2021**, *246*, 107617. [CrossRef]

54. Fellinger, J.; Citarella, R.; Giannella, V.; Lepore, M.; Sepe, R.; Czerwinski, M.; Herold, F.; Stadler, R. Overview of fatigue life assessment of baffles in Wendelstein 7-X. *Fusion Eng. Des.* **2018**, *136*, 292–297. [CrossRef]

55. Armentani, E.; Caputo, F.; Esposito, L.; Giannella, V.; Citarella, R. Multibody Simulation for the Vibration Analysis of a Turbocharged Diesel Engine. *Appl. Sci.* **2018**, *8*, 1192. [CrossRef]

56. Ovchinnikov, D.; Pokatsky, V.; Gallyamov, D. Factors affecting the dynamic rail canting of the railway track. *Transp. Res. Procedia* **2021**, *54*, 544–551. [CrossRef]

57. Ovchinnikov, D.V.; Pokatsky, V.A.; Gallyamov, D.I. Determination of the modulus of elasticity of the under-rail foundation of a railway track by the finite element method. *Transp. Infrastruct. Sib. Reg.* **2019**, *1*, 585–591.

58. Ovchinnikov, D.V.; Pokatskiy, V.A. Determination of the stress-strain state of the main site of the subgrade depending on the thickness of the ballast layer and sand cushion at different axle loads. *Sci. Educ. Transp.* **2016**, *2*, 76–180.

59. Menetrey, P.; Willam, K.J. Triaxial failure criterion for concrete and its generalization. *ACI Struct. J.* **1995**, *92*, 311–318.